nature chemistry

ARTICLES

PUBLISHED ONLINE: 6 MARCH 2011 | DOI: 10.1038/NCHEM.1005

Gradient-driven motion of multivalent ligand molecules along a surface functionalized with multiple receptors

András Perl[1], Alberto Gomez-Casado[1], Damien Thompson[2], Henk H. Dam[1], Pascal Jonkheijm[1], David N. Reinhoudt[1] and Jurriaan Huskens[1]*

The kinetics of multivalent (multisite) interactions at interfaces is poorly understood, despite its fundamental importance for molecular or biomolecular motion and molecular recognition events at biological interfaces. Here, we use fluorescence microscopy to monitor the spreading of mono-, di- and trivalent ligand molecules on a receptor-functionalized surface, and perform multiscale computer simulations to understand the surface diffusion mechanisms. Analogous to chemotaxis, we found that the spreading is directional (along a developing gradient of vacant receptor sites) and is strongly dependent on ligand valency and concentration of a competing monovalent receptor in solution. We identify multiple surface diffusion mechanisms, which we call walking, hopping and flying. The study shows that the interfacial behaviour of multivalent systems is much more complex than that of monovalent ones.

Molecular motion is at the heart of all biological and chemical processes, and molecular-scale devices will rely on harnessing its fundamental properties[1,2]. Mechanisms have been investigated that link molecular to macroscopic motion in biological systems[3], allowing the implementation of biological molecular motors in artificial systems[4,5]. Fully synthetic systems have also been designed with the specific aim of controlling motion at the molecular level[6–12]. In biology, motion occurs on all relevant lengthscales, ranging from molecular and cellular motion to the motion of complete organisms. At the cellular level, an individual cell may experience osmotic stress, which may influence its motion[13]. Alternatively, it may be subject to a gradient, for example in the concentration of a chemical in the surrounding solution or at an interface[14–16], which induces an attractive or repulsive motion of the cell, called chemotaxis. Whereas chemotaxis is an active response of the cell to a gradient, molecular motion is expected to be passive and driven by downhill energetic processes. The control of molecular motion by chemical gradients is still in its infancy[17–19].

Multivalent (multisite) interactions at interfaces play a pivotal role in many biological phenomena[20,21], including dynamic processes such as interfacial recognition and endocytosis. The thermodynamics of multivalent interactions at interfaces is relatively well understood[22–24]. However, it remains a formidable task to provide a kinetic understanding of multivalent systems. Very few quantitative studies on the kinetics of multivalent systems exist[25,26], and kinetic studies of multivalent interactions at interfaces are completely lacking. Here, we study the interfacial diffusion of multivalent ligand molecules along a receptor-functionalized surface. We show that a gradient of free receptor sites plays an accelerating role in the diffusion. The underlying complexity of the surface diffusion mechanisms is elucidated.

Results and discussion

In the present studies, the multivalent interfaces are monolayers of β-cyclodextrin (CD) receptor molecules covalently attached to glass substrates. Such surfaces constitute a powerful model system with which to quantitatively study multivalent interactions at interfaces, because of the uniformity and accessibility of the surface receptor sites and the relative ease of local functionalization by non-covalent patterning[24].

To study the effect of valency on the surface diffusion of molecules, mono- ($\mathbf{G^I}$), di- ($\mathbf{G^{II}}$) and trivalent ($\mathbf{G^{III}}$) ligand guest molecules (Fig. 1a) were prepared, with adamantane (Ad) moieties for binding to the CD receptors, a lissamine rhodamine B label for fluorescence detection, and flexible tetraethylene glycol spacers for water solubility and efficient multivalent binding. The guest molecules were assembled onto the CD-functionalized substrates by microcontact printing followed by rinsing with water, resulting in lines with an edge roughness below the diffraction limit. In the dry state, printed patterns (Fig. 2a) were stable in time and intensity[27]. In the present experiments, samples were covered with a known volume of water in the absence or presence of varying concentrations of free CD host in solution ('liquid', $\mathbf{H_l}$). Adding the monovalent $\mathbf{H_l}$ induces competition for binding of the Ad moieties to the multivalent CD receptor ('solid', $\mathbf{H_s}$) surface, leading to an apparent weakening of the multivalent interaction at the surface[27]. Figure 1b shows thermodynamic equilibria between the various guest species in solution and at the surface for $\mathbf{G^{II}}$. Spreading of the adsorbed guest molecules away from the original contact areas is used as a signature to study surface diffusion.

Spreading in time was monitored by fluorescence microscopy imaging of the line patterns. The intensities of the lines were averaged to obtain the peak maximum intensity difference, ΔI, and the peak width at half maximum, w (Fig. 2a). Figure 2b presents a typical selection of images for printed patterns of $\mathbf{G^{II}}$ in a solution of 2 mM CD. The sequence of images and integrated line intensities clearly shows line broadening and spreading in time, as qualitatively indicated by the 'blurring' of the lines and the decrease in maximum peak intensities.

To gain insight into the competition by $\mathbf{H_l}$, initial spreading rates (r) of $\mathbf{G^I}$–$\mathbf{G^{III}}$ were plotted as a function of the total concentration of

[1]Molecular Nanofabrication Group, MESA+ Institute for Nanotechnology, University of Twente, PO Box 217, 7500 AE Enschede, The Netherlands, [2]Tyndall National Institute, University College Cork, College Road, Cork, Ireland. *e-mail: j.huskens@utwente.nl

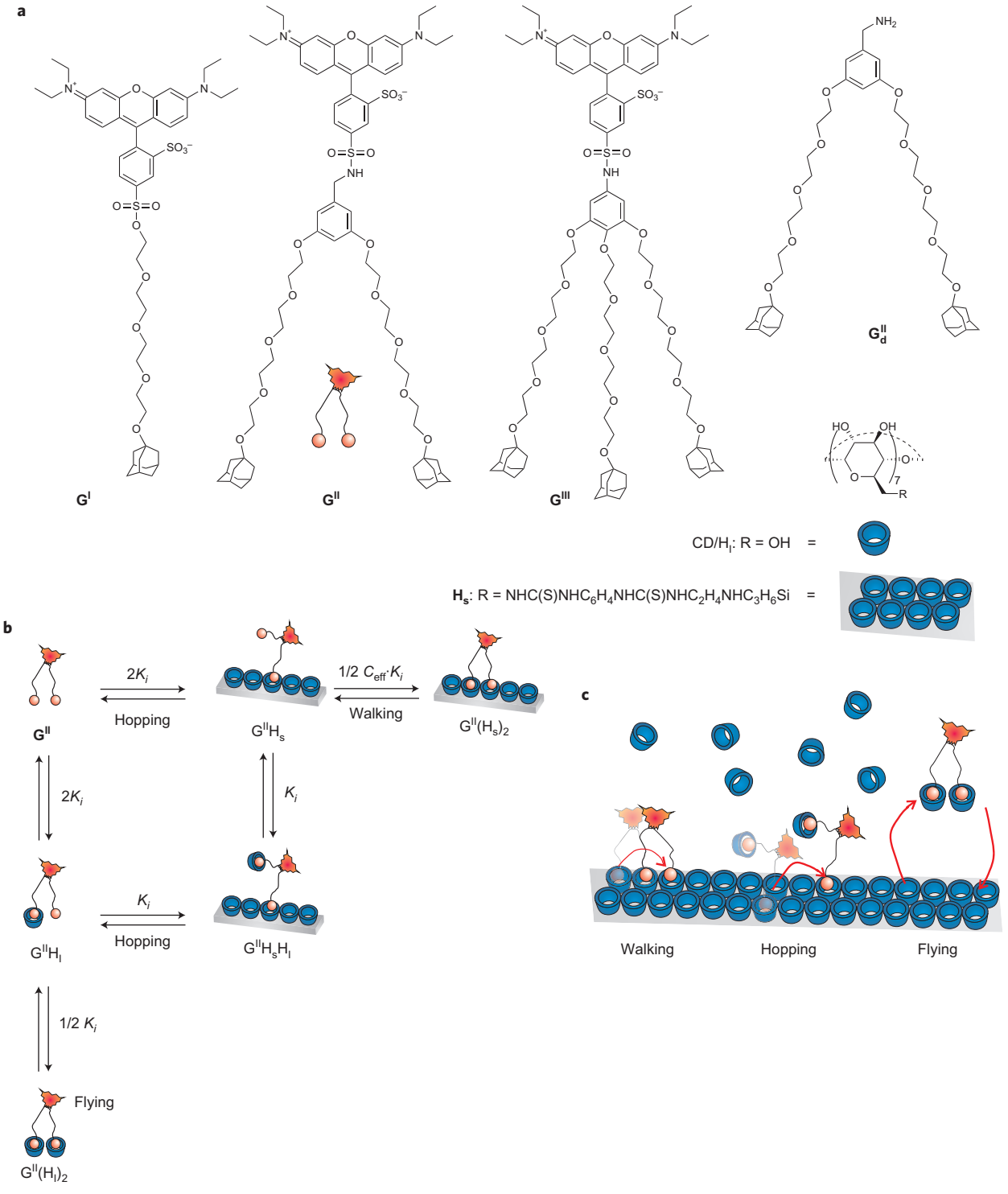

Figure 1 | Guest and host compounds, divalent thermodynamic equilibria and kinetic pathways. a, Chemical structures of guest (G) and host (H) compounds. **b**, Equilibria for divalent guest $\mathbf{G^{II}}$ binding to surface host $\mathbf{H_s}$ and solution host $\mathbf{H_I}$, with indications of stability constants (derived as described in ref. 22) and surface diffusion mechanisms (for monovalent and trivalent examples, see Supplementary Fig. S4). **c**, Cartoon of the basic mechanisms involved in multivalent surface diffusion.

$\mathbf{H_I}$, $[\mathbf{H_I}]_{tot}$ (Fig. 2c; see Supplementary Information for details about the spreading experiments). For monovalent $\mathbf{G^I}$, the spreading rate in pure water was already considerable (0.9 nm s^{-1}), and it rapidly increased following the addition of $\mathbf{H_I}$. On the other hand, desorption occurred (the point at which desorption begins is estimated from the ΔI_{max} versus time plots; see Supplementary Information) at any concentration of $\mathbf{H_I}$, even in pure water, as expected from the reversible binding nature of $\mathbf{G^I}$. Therefore, spreading rates could only be determined up to $[\mathbf{H_I}]_{tot} = 0.2$ mM. Most remarkable is the plot of r versus $[\mathbf{H_I}]_{tot}$ for the divalent $\mathbf{G^{II}}$: r initially increases with an increase in $[\mathbf{H_I}]_{tot}$ (up to $[\mathbf{H_I}]_{tot} = 0.8$ mM), then decreases (until $[\mathbf{H_I}]_{tot} = 1.5$ mM), and then increases again at higher $[\mathbf{H_I}]_{tot}$. The occurrence of such distinct phases in the spreading process is a sign of different spreading mechanisms prevailing at different $[\mathbf{H_I}]_{tot}$.

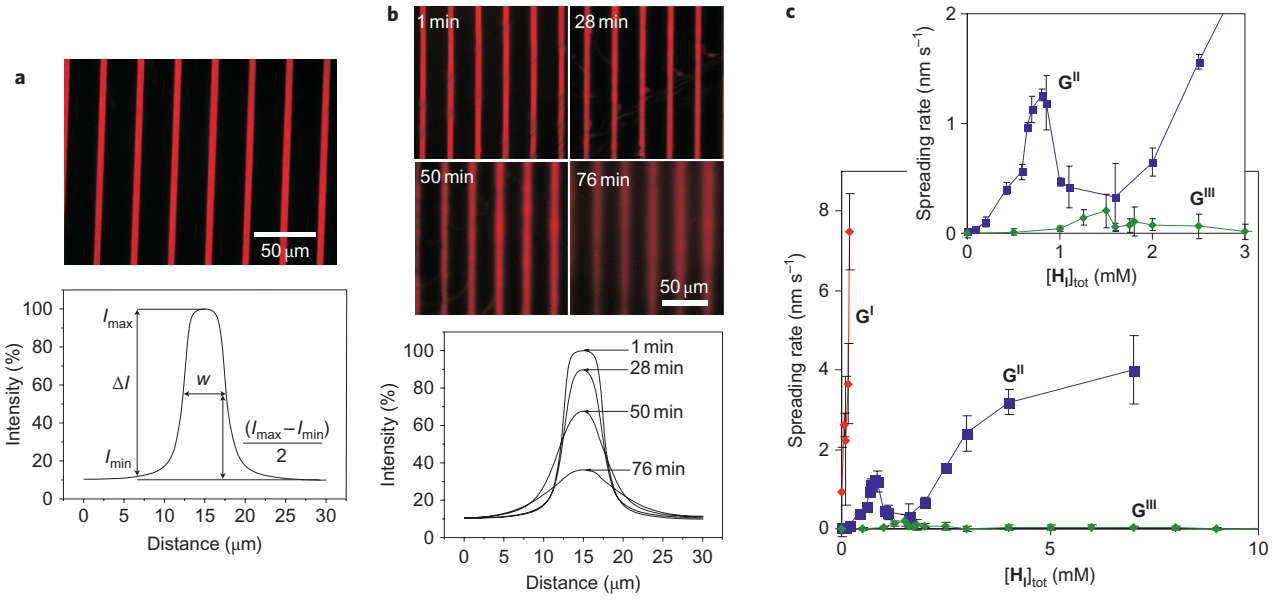

Figure 2 | Evaluation of spreading rates. a, Fluorescence microscopy image of $\mathbf{G^{II}}$ patterned in 5 μm lines on an $\mathbf{H_s}$ receptor surface created by microcontact printing (top); line profile averaged over the whole image perpendicular to the lines (bottom), with parameters w (full peak width at half maximum) and ΔI (intensity difference at peak maximum) being used to define spreading. **b**, Fluorescence microscopy images (top) and integrated line profiles (bottom) of $\mathbf{G^{II}}$ on a printed $\mathbf{H_s}$ surface after incubation for given amounts of time in a solution with 2 mM CD ($\mathbf{H_l}$). **c**, Spreading rates r (defined as initial slopes $(\partial w/\partial t)_0$ in a plot of w versus time t) as a function of $[\mathbf{H_l}]_{tot}$ in a solution used for incubating printed samples of $\mathbf{G^I}$, $\mathbf{G^{II}}$ and $\mathbf{G^{III}}$ (error bars represent a single standard deviation over three or more independently performed measurements at each $[\mathbf{H_l}]_{tot}$ concentration). Inset: magnification of the low concentration range for $\mathbf{G^{II}}$ and $\mathbf{G^{III}}$ to more clearly show the maxima in spreading rates observed for these guests.

Desorption began to become apparent only at $[\mathbf{H_l}]_{tot} = 1$ mM, rapidly gaining in importance at $[\mathbf{H_l}]_{tot} > 2$ mM. The spreading rate in pure water (0.02 nm s^{-1}) was about two orders of magnitude lower than for $\mathbf{G^I}$. The trivalent $\mathbf{G^{III}}$ only showed values of r significantly larger than 0 in the range $[\mathbf{H_l}]_{tot} = 1$–2 mM, with a maximum at ~1.5 mM. No desorption was observed at any $[\mathbf{H_l}]_{tot}$.

At thermodynamic equilibrium, the apparent binding affinity of a multivalent molecule is dependent on the surface concentration of free, uncomplexed receptor sites, which is described by the effective concentration C_{eff} (ref. 22). In the experiments described above, C_{eff} (and therefore also the binding affinity) is relatively low in the printed areas and high in the uncovered areas. Thus a gradient of C_{eff} is established, which is steep directly after printing and becomes less steep over time, during spreading. To assess the effect of this developing gradient on spreading rate, patterned substrates with printed $\mathbf{G^{II}}$ were put in a solution of the also divalent but non-fluorescent ('dark') $\mathbf{G^{II}_d}$ (Fig. 1a) to backfill the non-printed areas. On such substrates, C_{eff} is expected to be constant in time and place, thus eliminating the effect of the gradient.

In pure water, the spreading rates of the backfilled samples were indistinguishable from the printed-only samples. In contrast, in the presence of competitor ($[\mathbf{H_l}]_{tot} = 0.8$ mM), the spreading rate of the printed-only samples was relatively high (1.3 nm s^{-1}; Fig. 2c), and the spreading rates for backfilled samples (Supplementary Fig. S3) were significantly lower (0.2 and 0.3 nm s^{-1} for samples with 100 and 40% coverage, respectively). For the printed-only samples, the spreading rate remained high and constant, with ΔI dropping from 100% to ~40% of the initial intensity, indicating that the change in coverage during spreading is not an explanation for the observed difference in spreading rates between the printed-only and backfilled samples. The difference in spreading rate therefore indicates that random spreading, observed for the backfilled samples, is only 15–25% of the spreading rate observed for the printed-only samples. This proves that the spreading at the printed-only surfaces is directional and gradient-driven.

In the case of monovalent $\mathbf{G^I}$, three guest species exist: the unbound solution species $\mathbf{G^I}$, the species G^IH_l associated with a CD from solution, and the surface-bound G^IH_s (Supplementary Fig. S4a). Both the spreading (Fig. 2c) and the apparent desorption are strongly enhanced by the addition of $\mathbf{H_l}$. This addition of $\mathbf{H_l}$ leads to an increase in the concentration of G^IH_l, with a concomitant decrease of the equilibrium concentrations of both $\mathbf{G^I}$ and G^IH_s. This suggests that the enhanced spreading and desorption rates at increased $[\mathbf{H_l}]_{tot}$ can be attributed to the free diffusion ('flying') of G^IH_l. Measurable spreading can only be observed when laterally diffused species readsorb, which has to be preceded by the relatively slow dissociation step of G^IH_l to $\mathbf{G^I}$ to create a free Ad moiety. Therefore G^IH_l has a relatively long lifetime and a high probability of diffusing into the bulk before readsorption can occur. The dependence on $[\mathbf{H_l}]_{tot}$ also shows that spreading and desorption are rate-limited by diffusion of G^IH_l into the bulk, rather than by the intrinsic dissociation of surface-adsorbed G^IH_s. This view is confirmed by a comparison of the intrinsic (un)binding rate constants of CD complexes and mass transport (see Supplementary Information for mass transport considerations), which indicates that the concentrations of $\mathbf{G^I}$ and G^IH_l near the surface are in (local) equilibrium with G^IH_s, so thermodynamic equilibrium models can be used to predict trends of concentrations of different solution and surface species and their relative roles at different stages of the spreading process.

In pure water in the absence of $\mathbf{H_l}$, however, spreading and desorption have to occur via the solution species $\mathbf{G^I}$. Because reassociation of an uncapped Ad moiety is very fast, rebinding is likely and therefore occurs many times before the species gets the chance to move far enough from the surface to diffuse into the bulk. Obviously, there is a chance that this rebinding will not occur at the same receptor site but at a neighbouring free site, which is the underlying mechanism of spreading at this stage. The distance that can be travelled in the unbound state is dependent on the lifetime of the species. Assuming a diffusion constant of

$D \approx 1 \times 10^{-10}$ m^2 s^{-1} and a lifetime of ~0.1 μs, an average travelling distance of only a few nanometres is found, which indicates that only nearby receptor sites are within reach (the distance between neighbouring $\mathbf{H_s}$ sites is 2 nm). This mechanism is therefore called 'hopping', because it most closely resembles the hopping of individual atoms on a metal surface[28,29].

The more complex spreading behaviour of the divalent $\mathbf{G^{II}}$ (Fig. 2c) indicates the coexistence of different spreading mechanisms (Fig. 1c). Six different guest species exist for this system (Fig. 1b). The observed spreading rate increase at $[\mathbf{H_l}]_{tot} > 1.5$ mM (Fig. 2c) occurs simultaneously with apparent desorption. The spreading in this regime is therefore attributed to an increase in the concentration of the fully capped $G^{II}(H_l)_2$. Similar to $G^{I}H_l$ in the monovalent case, this is a long-lived species and thus travels farther than any uncapped species, both along the surface and into the bulk.

In the absence of $\mathbf{H_l}$, two mechanisms seem plausible (Fig. 1b, top row): hopping of the species $\mathbf{G^{II}}$ (similar to hopping of $\mathbf{G^{I}}$ in the monovalent case), and a mechanism in which the guest molecule remains bound at the surface via at least one Ad moiety, coined 'walking'. The latter is only possible for multivalent molecules. Equilibrium calculations show that the near-surface concentrations of the species involved in hopping ($\mathbf{G^{II}}$ and $G^{II}H_s$; Fig. 3a,b) are three orders of magnitude lower than for the corresponding species in the monovalent case ($\mathbf{G^{I}}$ and $G^{I}H_s$; Supplementary Fig. S5a,b), whereas the spreading rate is only a factor of 50 lower. The relatively high spreading rate, and the higher concentrations of the species associated with the walking pathway, therefore indicate that the walking pathway is the preferred one in pure water.

As $[\mathbf{H_l}]_{tot}$ increases from 0 to 0.8 mM, an increase is observed in the spreading rate (Fig. 2c), together with a decrease in the concentrations of both $G^{II}H_s$ and $G^{II}(H_s)_2$ (which are associated with walking; Fig. 3a,b). The rate enhancement and absence of desorption in this range therefore indicate that hopping has become dominant over walking. The accelerating increase in the spreading rate in the range $0 < [\mathbf{H_l}]_{tot} < 0.5$ mM supports this transition of mechanisms. At the $\mathbf{H_l}$ concentrations used here, the CD-capped species $G^{II}H_sH_l$ and $G^{II}H_l$ are one to two orders of magnitude more abundant than the corresponding uncapped species $G^{II}H_s$ and $\mathbf{G^{II}}$ (Fig. 3a,b). Thus, an increase in $[\mathbf{H_l}]_{tot}$ leads to rapid population of the capped species, and their hopping is the dominant spreading mechanism.

Finding an explanation for the observed decrease in the spreading rate at $0.8 < [\mathbf{H_l}]_{tot} < 1.5$ mM (Fig. 2c) remains challenging. The concentrations of the main species involved in the hopping pathway level off in this range (Fig. 3a,b), but do not decrease upon further addition of $\mathbf{H_l}$, which indicates that the observed decrease in the spreading rate cannot be explained only by the concentration trends. It is most likely that a transition occurs from the hopping to the flying mechanism; this is supported by the observed desorption in this range. One plausible explanation could be a growing fraction of molecules entering the bulk (by full dissociation and capping to give $G^{II}(H_l)_2$) at the onset of desorption. This would initially reduce the near-surface concentrations of the species causing spreading, until the concentration of $G^{II}(H_l)_2$ becomes so high that this species itself becomes the main spreading contributor at $[\mathbf{H_l}]_{tot} > 1.5$ mM.

In an alternative explanation, the relative probabilities are considered for rebinding of an uncapped Ad moiety of the main hopping species $G^{II}H_l$ at the same receptor site (unsuccessful event) or at a neighbouring free receptor site (successful event) (Fig. 3c). An increase in $[\mathbf{H_l}]$ promotes the formation of $G^{II}(H_l)_2$, and so decreases the lifetime of $G^{II}H_l$ and therefore enhances the probability of an unsuccessful hopping event relative to a successful event. Because the lifetime of this species is so short that it is only able to reach neighbouring receptor sites (see above), this supports the idea that a further reduction of the lifetime can have a drastic

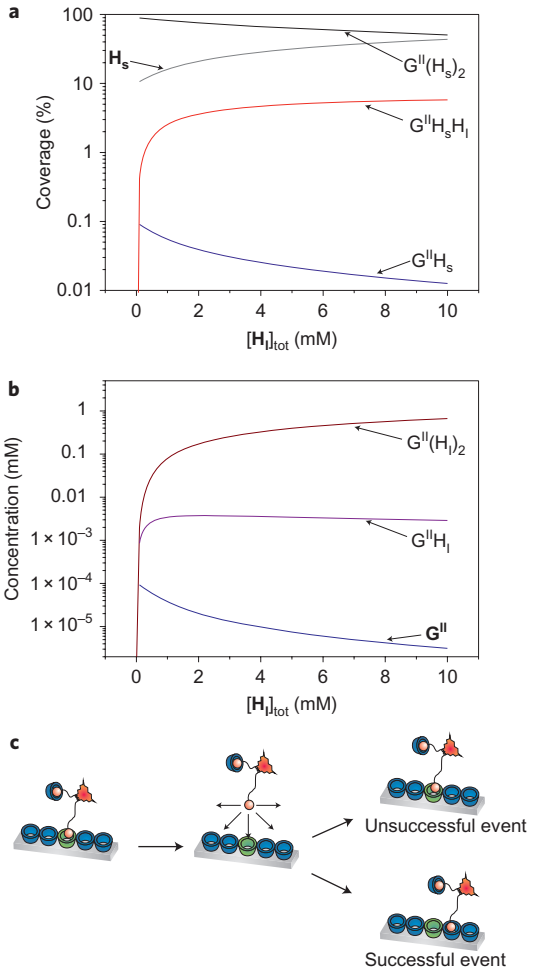

Figure 3 | Themodynamic equilibrium concentrations and representation of rebinding probability. a,**b**, Thermodynamic equilibrium concentrations of surface (**a**) and solution (**b**) species of the divalent $\mathbf{G^{II}}$, assuming an initial guest coverage of 90%. **c**, Divalent species $G^{II}H_sH_l$ involved in a hopping sequence: dissociation to $G^{II}H_l$ followed by rebinding at the same position (unsuccessful event) or at a neighbouring vacant $\mathbf{H_s}$ site (successful event).

effect on the ratio between successful and unsuccessful hopping events in favour of the latter. This explanation is supported by the similar decrease in spreading rate observed (see below) for $\mathbf{G^{III}}$, which does not desorb and hence cannot fly into the bulk.

The experiments and thermodynamic equilibrium calculations are supported by molecular simulations. Previous molecular dynamics (MD) computer simulations[30–32] revealed the mechanisms by which both the individual guest–CD interactions and collective multivalent ligand–surface interactions may be tuned by molecular design and also by changing the assembly conditions (for example, pH and temperature). Our new MD simulations (see Supplementary Information) show that the multivalent guest molecules can only access neighbouring CD cavities. Most importantly, both partially and fully uncomplexed molecules are initially kept at a subnanometre distance from the surface, with the same polar interactions that provide the close contact also biasing the path of unbinding of a dissociated Ad group towards the surface cavity it was released from, confirming a relatively high probability for rebinding at the same position.

In addition to the MD simulations, a nanoscale Monte Carlo simulation of the multivalent surface and the covering solution was developed to study the evolution of $\mathbf{G^{II}}$ species at the surface and in solution at the molecular level (Fig. 4). A clear

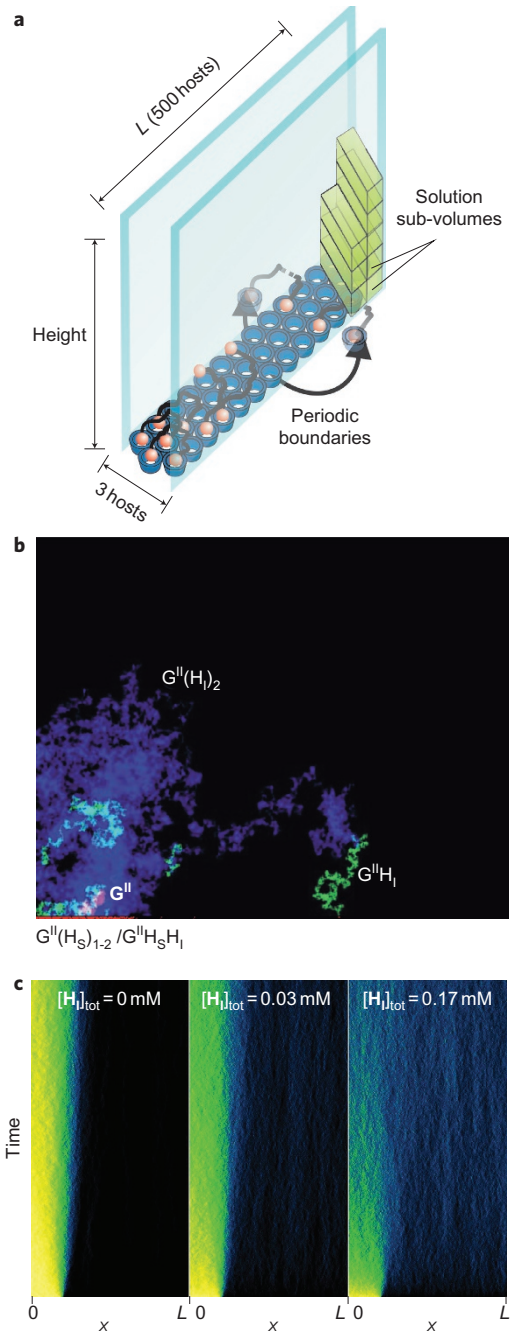

Figure 4 | Monte Carlo simulations. a, Setup of a Monte Carlo simulation showing a slice (three $\mathbf{H_s}$ sites wide) with a compartmentalized solution on top. Periodic boundary conditions provide the extended surface. **b**, Representative species distribution obtained during the simulation, indicating guest species at the surface and in solution. **c**, Time traces of simulations showing only the surface species, and an evolution in time as a function of $[\mathbf{H_l}]_{tot}$ in solution.

dependence of spreading rate on the concentration of $\mathbf{H_l}$ is shown. Evolution of the bound guest on the surface was fitted as a one-dimensional diffusion process to yield an apparent diffusion constant (Supplementary Fig. S9), which increased with increasing $\mathbf{H_l}$ concentration. Modulation of the height of the solution over the surface revealed a volume-independent spreading in the case of low $\mathbf{H_l}$ concentration ($[\mathbf{H_l}]_{tot} < 0.5$ mM). This behaviour indicates that a locally restricted mechanism (hopping) is responsible for the spreading. However, at ~0.8 mM, a transition to a volume-dependent regime occurred, in agreement with an in-bulk mechanism (flying) becoming the main mode of spreading.

In the case of trivalent $\mathbf{G^{III}}$, spreading was much slower and only observed in a rather small range of $\mathbf{H_l}$ concentrations (Fig. 2c), whereas desorption was completely absent at any $[\mathbf{H_l}]_{tot}$. Ten guest species exist, with various options for walking and hopping (Supplementary Fig. S4b). Walking of $G^{III}(H_s)_3$ (in pure water) was too slow to be measured. The apparent increase of spreading rate at $1.0 < [\mathbf{H_l}]_{tot} < 1.5$ mM can potentially be attributed to an increase in hopping of $G^{III}H_s(H_l)_2$ and walking of $G^{III}(H_s)_2H_l$. However, the latter is unlikely, because the concentrations of the species involved in walking ($G^{III}(H_s)_2H_l$ and $G^{III}H_sH_l$) were much lower compared to the corresponding concentrations of the walking species in the divalent case ($G^{II}(H_s)_2$ and $G^{II}H_s$), and the actual spreading rates observed in this range for the trivalent case were higher than the walking rate observed in the divalent system (as observed at $[\mathbf{H_l}]_{tot} = 0$). This therefore indicates a preference for the hopping pathway. The decrease of spreading rate at $[\mathbf{H_l}]_{tot} > 1.5$ mM is attributed to an increase in the probability for rebinding at the same receptor site, as discussed above for the divalent case.

The affinity (K_i) and kinetics of the individual host–guest interaction, here CD–Ad, can be altered by (i) changing the guest moiety, (ii) changing the temperature, and (iii) changing the solvent polarity. Only the last option was tried here, and spreading of $\mathbf{G^{II}}$ was studied in 10% (v/v) methanol in water, without CD in solution. A 10 times higher spreading rate was observed compared to pure water. At a decreased affinity, one expects an increase of the intrinsic dissociation rate constant and a concomitant increase of the equilibrium concentration of the walking species $G^{II}H_s$. The observed spreading rate increase can therefore be attributed to a threefold decrease in K_i, which is, within experimental error, equal to the observed twofold decrease. More importantly, this experiment qualitatively shows that the surface diffusion rates of multivalent ligands may drastically alter with a change in K_i, which suggests opportunities for changing and tuning spreading rates through molecular design.

Conclusions

We have shown that the complex spreading behaviour observed for multivalent ligands is gradient-driven, and that several mechanisms underpin the observed spreading. These mechanisms are supported by thermodynamic equilibrium models and both MD and Monte Carlo simulations. Molecular understanding of the kinetics of multivalent interactions on surfaces offers an improved insight into interfacial recognition processes, for example, as models for biological cell membranes, and offers potentially new strategies for the design of molecular-based devices. Future research directions could include the further development of switchable ligands featuring multiple recognition sites, which might find use in molecular medicine and molecular electronic devices.

Methods

Assembly of dye guests on CD substrates. Monolayers of β-cyclodextrin (CD) on glass were prepared in four steps, using a method developed previously by our group[27]. Microcontact printing was used to pattern the CD monolayers on glass with fluorescent dyes. Stamps were prepared from commercially available Sylgard-184 poly(dimethyl siloxane) (Dow Corning). The curing agent and prepolymer were manually mixed in a 1:10 volume ratio and cured overnight at 60 °C against the master. The cured stamp was peeled off from the master at the curing temperature. Silicon masters with 5-μm-wide line features with a separation of 25 μm were fabricated by photolithography. This high spacing/feature ratio was necessary to ensure a large enough free spreading space for the guest molecules during measurements, and for easy data transformation.

The stamps were mildly oxidized in an oxygen plasma reactor before use. Before printing, the stamps were inked by soaking them in an aqueous solution of the fluorescent dye (~10 μM). After drying the surface of the stamps with nitrogen, conformal contact was achieved manually. The stamps were weakly pressed against the printboard surface at the initial stage of printing to induce conformal contact.

The printing time in all cases was 1 min. The samples with the patterned self-assembled monolayers of the guest were rinsed immediately after printing with a continuous flow of pure water ($\mathbf{G^{I}}$, 10 s; $\mathbf{G^{II}}$ and $\mathbf{G^{III}}$, 30 s) to remove the physisorbed molecules, then dried in a stream of nitrogen.

Backfilling with $\mathbf{G_d^{II}}$ was achieved by immersion of the samples in a 0.1 mM aqueous solution of $\mathbf{G_d^{II}}$ for 10 s. Low coverage (40%) of the mixed divalent SAM was achieved by rinsing with 20% ethanol in water for 30 s, and measured using fluorescence intensities.

Spreading experiments. Aqueous solutions (280 μl) containing 0–12 mM CD were applied on top of the patterned surface, confined by a rubber ring with a diameter of 11.6 mm. The printboard surface/rubber ring/liquid system was immediately covered with a clean glass slide to close the volume and to avoid evaporation. A thin layer of vacuum grease on the rubber ring was used to stick the solid components together.

Fluorescence micrographs were taken frequently. To avoid the effect of photobleaching, new areas were selected after each shot. The focusing time before taking the micrographs was 20 s in all cases. For faster focusing, the analysed spot was irradiated further until the 20 s time period was reached. Imaging was continued as long as the intensity difference between the dark and bright areas allowed proper focusing and reliable assessment of ΔI.

Fluorescent images were taken using an Olympus inverted research microscope (IX71) equipped with a mercury burner (U-RFL-T) as a light source and a digital camera Olympus DP70 (12.5-million-pixel cooled digital colour camera) for image acquisition. Green excitation light ($510\ \text{nm} \leq \lambda \leq 550\ \text{nm}$) and red emission light ($\lambda > 590\ \text{nm}$) were filtered using a U-MWG Olympus filter cube.

Received 18 August 2010; accepted 1 February 2011; published online 6 March 2011

References

1. Thibault-Starzyk, F., Seguin, E., Thomas, S. Daturi, M., Arnolds, H. & King, D. A. Real-time infrared detection of cyanide flip on silver-alumina NO_x removal catalyst. *Science* **324,** 1048–1051 (2009).
2. Backus, E. H. G., Eichler, A., Kleyn, A. W. & Bonn, M. Real-time observation of molecular motion on a surface. *Science* **310,** 1790–1793 (2005).
3. Helenius, J., Brouhard, G., Kalaidzidis, Y., Diez, S. & Howard, J. The depolymerizing kinesin MCAK uses lattice diffusion to rapidly target microtubule ends. *Nature* **441,** 115–119 (2006).
4. Hess, H., Clemmens, J., Qin, D., Howard, J. & Vogel, V. Light-controlled molecular shuttles made from motor proteins carrying cargo on engineered surfaces. *Nano Lett.* **1,** 235–239 (2001).
5. Goel, A. & Vogel, V. Harnessing biological motors to engineer systems for nanoscale transport and assembly. *Nature Nanotech.* **3,** 465–475 (2008).
6. Gu, H., Chao, J., Xiao, S.-J. & Seeman, N. C. A proximity-based programmable DNA nanoscale assembly line. *Nature* **465,** 202–205 (2010).
7. Lund, K. *et al.* Molecular robots guided by prescriptive landscapes. *Nature* **465,** 206–210 (2010).
8. Von Delius, M., Geertsema, E. M. & Leigh, D. A. A synthetic small molecule that can walk down a track. *Nature Chem.* **2,** 96–101 (2010).
9. Berna, J. *et al.* Macroscopic transport by synthetic molecular machines. *Nat. Mater.* **4,** 704–710 (2005).
10. Kelly, T. R. Molecular motors: synthetic DNA-based walkers inspired by kinesin. *Angew. Chem. Int. Ed.* **44,** 4124–4127 (2005).
11. Badjic, J. D., Balzani, V., Credi, A., Silvi, S. & Stoddart, J. F. A molecular elevator. *Science* **303,** 1845–1849 (2004).
12. Feringa, B. L. In control of motion: from molecular switches to molecular motors. *Acc. Chem. Res.* **34,** 504–513 (2001).
13. Sakai, N. & Matile, S. G-quartet self-assembly under osmotic pressure: remote control by vesicle shrinking rather than stress. *Chirality* **15,** 766–771 (2003).
14. Servant, G. *et al.* Polarization of chemoattractant receptor signaling during neutrophil chemotaxis. *Science* **287,** 1037–1040 (2000).
15. Ueda, M., Sako, Y., Tanaka, T., Devreotes, P. & Yanagida, T. Single-molecule analysis of chemotactic signaling in dictyostelium cells. *Science* **294,** 864–867 (2001).
16. Kim, M. S., Khang, G. & Lee, H. B. Gradient polymer surfaces for biomedical applications. *Prog. Polym. Sci.* **33,** 138–164 (2008).
17. Chang, T., Rozkiewicz, D. I., Ravoo, B. J., Meijer, E. W. & Reinhoudt, D. N. Directional movement of dendritic macromolecules on gradient surfaces. *Nano Lett.* **7,** 978–980 (2007).
18. Burgos, P., Zhang, Z., Golestanian, R., Leggett, G. J. & Geoghegan, M. Directed single molecule diffusion triggered by surface energy gradients. *ACS Nano* **3,** 3235–3243 (2009).
19. Tauk, L., Schroder, A. P., Decher, G. & Giuseppone, N. Hierarchical functional gradients of pH-responsive self-assembled monolayers using dynamic covalent chemistry on surfaces. *Nature Chem.* **1,** 649–656 (2009).
20. Kiessling, L. L., Gestwicki, J. E. & Strong, L. E. Synthetic multivalent ligands as probes of signal transduction. *Angew. Chem. Int. Ed.* **45,** 2348–2368 (2006).
21. Mammen, M., Choi, S. K. & Whitesides, G. M. Polyvalent interactions in biological systems: implications for design and use of multivalent ligands and inhibitors. *Angew. Chem. Int. Ed.* **37,** 2754–2794 (1998).
22. Huskens, J. *et al.* A model for describing the thermodynamics of multivalent host–guest interactions at interfaces. *J. Am. Chem. Soc.* **126,** 6784–6797 (2004).
23. Houseman, B. T. & Mrksich, M. Model systems for studying polyvalent carbohydrate binding interactions, in *Host–Guest Chemistry: mimetic approaches to study carbohydrate recognition* (Topics in Current Chemistry) Vol. 218 (ed. Penades, S.) 1–44 (Springer, 2002).
24. Ludden, M. J. W., Reinhoudt, D. N. & Huskens, J. Molecular printboards: versatile platforms for the creation and positioning of supramolecular assemblies and materials. *Chem. Soc. Rev.* **35,** 1122–1134 (2006).
25. Rao, J. H., Lahiri, J., Isaacs, L., Weis, R. M. & Whitesides, G. M. A trivalent system from vancomycin-D-Ala-D-Ala with higher affinity than avidin–biotin. *Science* **280,** 708–711 (1998).
26. Badjić, J. D., Cantrill, S. J. & Stoddart, J. F. Can multivalency be expressed kinetically? The answer is yes. *J. Am. Chem. Soc.* **126,** 2288–2289 (2004).
27. Onclin, S., Mulder, A., Huskens, J., Ravoo, B. J. & Reinhoudt, D. N. Molecular printboards: monolayers of β-cyclodextrins on silicon oxide surfaces. *Langmuir* **20,** 5460–5466 (2004).
28. Antczak, G. & Ehrlich, G. Jump processes in surface diffusion. *Surf. Sci. Rep.* **62,** 39–61 (2007).
29. Hla, S.-W. Scanning tunneling microscopy single atom/molecule manipulation and its application to nanoscience and technology. *J. Vac. Sci. Technol. B* **23,** 1351–1360 (2005).
30. Thompson, D. & Larsson, J. A. Modeling competitive guest binding to β-cyclodextrin molecular printboards. *J. Phys. Chem. B* **110,** 16640–16645 (2006).
31. Thompson, D. Free energy balance predicates dendrimer binding multivalency at molecular printboards. *Langmuir* **23,** 8441–8451 (2007).
32. Cieplak, M. & Thompson, D. Coarse-grained molecular dynamics simulations of nanopatterning with multivalent inks. *J. Chem. Phys.* **128,** 234906 (2008).

Acknowledgements

This research was supported by the European FP6 Integrated project NaPa (A.P., H.D., J.H.; contract no. NMP4-CT-2003-500120) and by the Nanotechnology network in the Netherlands NanoNed (AGC; project no. TPC.6939). D.T. also acknowledges support from the European FP7 project FunMol (grant agreement no. 213382), Science Foundation Ireland (SFI) for computing resources at Tyndall National Institute and SFI/ Higher Education Authority for computing time at the Irish Centre for High-End Computing (ICHEC). The authors thank J. Opheusden for discussion of the Monte Carlo simulations.

Author contributions

A.P., A.G.C., P.J., D.N.R. and J.H. conceived and designed the experiments. A.P. and H.H.D. performed the experimental work. A.G.C. and D.T. performed the modelling. J.H. was responsible for the overall design, direction and supervision of the project. A.P., D.T., P.J., D.N.R. and J.H. co-wrote the paper.

Additional information

The authors declare no competing financial interests. Supplementary information and chemical compound information accompany this paper at www.nature.com/naturechemistry. Reprints and permission information is available online at http://npg.nature.com/reprintsandpermissions/. Correspondence and requests for materials should be addressed to J.H.